Supporting Information

Ion Polarisation-Assisted Hydrogen-Bonded Ferroelectrics in Liquid Crystalline Domain

Guohao Yuan, Yuko Kimura, Takayuki Kobayashi, Takashi Takeda, Norihisa Hoshino, and Tomoyuki Akutagawa*

Contents.

1. Experimental

General. The ^{1}H NMR spectra were recorded on a Bruker Avance 400 NMR spectrometer with the chemical shift (δ) in ppm relative to tetramethylsilane as a standard with δ = 0.00 ppm. The mass spectra were recorded on a JMS–700 spectrometer (MS laboratory, Graduate School of Agriculture, Tohoku University). Thermogravimetric (TG) differential thermal analysis and differential scanning calorimetry (DSC) were conducted using a Rigaku Thermo plus TG8120 thermal analysis station and Mettler DSC1-T with an Al_2O_3 reference and a heating and cooling rate of 5 K min^{-1} under nitrogen. Solid-state infrared (IR) spectra were measured on KBr pellets using a Thermo Fisher Scientific Nicolet 6700 spectrophotometer with a resolution of 5 cm^{-1}. Temperature-dependent powder X-ray diffraction (PXRD) profiles were obtained using a Rigaku Rint-Ultima diffractmeter with Cu Kα radiation with λ=1.54185 Å in the temperature range of 298−498 K. The temperature-dependent dielectric constants were measured by the two-probe AC impedance method from 1 kHz to 1 MHz (Hewlett-Packard, HP4194A) using the temperature controller of a Linkam LTS-E350 system. The cast film was fabricated on an ITO glass (SZ-A311P6N) and sandwiched using another ITO glass to form an electrode arrangement with an electrode area of 0.16 cm^2 and a gap ranging from 0.1 mm to 1.0 mm. The temperature was increased by 4 K min^{-1} in the corresponding temperature range. The *P–E* curves were measured using a ferroelectric tester (Precision LC, Radient Technologies).

Preparations. **3BC** was synthesized following a reported method.[55] Tetraamino-dibenzo[18]crown-6 was prepared according to a reported procedure.[56] Concentrated nitric acid (50 mL) was slowly dropped into dibenzo[18]crown-6 (5.0 g, 13.9 mmol) in CH_2Cl_2 (50 mL) at room temperature under stirring. Then, concentrated sulfuric acid (25 mL) was slowly dropped and stirred for four days. After filtration, the precipitate was washed with H_2O and dried in vacuum. Tetranitro-dibenzo[18]crown-6 (6.96 g, 12.9 mmol) was obtained with a yield of 93%. ^{1}H NMR in DMSO: δ = 3.85 (m, 8H), 4.31 (m, 8H), and 7.74 (s, 4H). Then, 10% Pd/C (1.0 g) and hydrazine monohydrate (140 mL) were added to tetranitro-dibenzo[18]crown-6 (4.6 g, 8.52 mmol) in dry C_2H_5OH, which was refluxed for 4 h under N_2. The hot reaction solution was filtered through celite with hot C_2H_5OH, and the solution was heated again and slowly cooled to obtain platelet crystals. Tetraamino-dibenzo[18]crown-6 (2.02 g, 4.75 mmol) was obtained with a yield of 56%. ^{1}H NMR in CD_3OD: δ = 3.91 (m, 8H), 4.08 (br, 8H), 6.48 (s, 4H).

Undecanoyl chloride (2.28 mL, 10.4 mmol) was slowly dropped into tetraamino-dibenzo[18]crown-6 in dry CH_3CN (80 mL) under N_2. Then, trimethylamine (2.56 mL, 18.4 mmol) was slowly dropped into the solution and stirred overnight. The white precipitate was collected by filtration, washed with CH_3OH, and dried in vacuum. Recrystallization from DMF provided 709 mg (0.648 mmol) of 1 with a yield of 27%. ^{1}H NMR: 400 MHz, $CDCl_3$, δ = 0.88 (9H, t), 1.21−1.43 (66H, m), 1.58−1.68 (6H, m), 3.38 (6H, dt), 6.40 (3H, t), 8.33 (3H, s). Anal. Calcd. for 3BC ($C_{51}H_{93}N_3O_3$): C, 76.92; H, 11.77; N, 5.28. Found: C, 76.82; H, 11.85; N, 5.30.

R1) Y. Shishido, H. Anetai, T. Takeda, N. Hoshino, S. –i. Noro, T. Nakamura, T. Akutagawa, Molecular assembly and ferroelectric response of benzenecarboxamides bearing multiple $-CONHC_{14}H_{29}$ Chains. *J. Phys. Chem. C.* **118**, 21204–21214 (2014).

R2) Y. P. Li, H. R. Yang, Q. Zhao, W. C. Song, J. Han, X. H. Bu, Ratiometric and selective fluorescent sensor for Zn^{2+} as an "Off-On-Off" switch and logic gate. *Inorg. Chem.* **51**, 9642–9648 (2012).

Tetraamino-dibenzo[18]crown-6 was prepared according to a reported procedure. Concentrated nitric acid (50 mL) was slowly dropped into dibenzo[18]crown-6 (5.0 g, 13.9 mmol) in CH_2Cl_2 (50 mL) at room temperature under stirring. Then, concentrated sulfuric acid (25 mL) was slowly dropped and stirred for four days. After filtration, the precipitate was washed with H_2O and dried in vacuum. Tetranitro-dibenzo[18]crown-6 (6.96 g, 12.9 mmol) was obtained with a yield of 93%. ^{1}H NMR in DMSO: $\delta = 3.85$ (m, 8H), 4.31 (m, 8H), and 7.74 (s, 4H). Then, 10% Pd/C (1.0 g) and hydrazine monohydrate (140 mL) were added to tetranitro-dibenzo[18]crown-6 (4.6 g, 8.52 mmol) in dry C_2H_5OH, which was refluxed for 4 h under N_2. The hot reaction solution was filtered through celite with hot C_2H_5OH, and the solution was heated again and slowly cooled to obtain platelet crystals. Tetraamino-dibenzo[18]crown-6 (2.02 g, 4.75 mmol) was obtained with a yield of 56%. ^{1}H NMR in CD_3OD: $\delta =$ 3.91 (m, 8H), 4.08 (br, 8H), 6.48 (s, 4H). Undecanoyl chloride (2.28 mL, 10.4 mmol) was slowly dropped into tetraamino-dibenzo[18]crown-6 in dry CH_3CN (80 mL) under N_2. Then, trimethylamine (2.56 mL, 18.4 mmol) was slowly dropped into the solution and stirred overnight. The white precipitate was collected by filtration, washed with CH_3OH, and dried in vacuum. Recrystallization from DMF provided 709 mg (0.648 mmol) of **1** with a yield of 27%. ^{1}H NMR: 400 MHz, $CDCl_3$, δ = 0.88 (9H, t), 1.21−1.43 (66H, m), 1.58−1.68 (6H, m), 3.38 (6H, dt), 6.40 (3H, t), 8.33 (3H, s). Anal. Calcd. for $C_{51}H_{93}N_3O_3$: C, 76.92; H, 11.77; N, 5.28. Found: C, 76.82; H, 11.85; N, 5.30. The ion-capturing M^+•(**1**)•X^- salts were obtained by simply mixing **1** in toluene and the corresponding M^+X^- salts in CH_3OH, followed by solvent removal under vacuum. Seven kinds of ion-doped salts, K^+•(**1**)•Br^-, K^+•(**1**)•I^-, K^+•(**1**)•PF_6^-, K^+•(**1**)•AcO^-, K^+•(**1**)•SCN^-, Na^+•(**1**)•PF_6^-, and Cs^+•(**1**)•$(CO_3^{2-})_{0.5}$, were obtained and their mixing states were evaluated by PXRD analysis. Mixed crystals, (**3BC**)$_{0.9}$(**1**)$_{0.1}$, (**3BC**)$_{0.8}$(**1**)$_{0.2}$, and (**3BC**)$_{0.7}$(**1**)$_{0.3}$ were obtained by simply mixing in hot toluene, removing the solvent under vacuum, and drying. Three kinds of ion-doped mixed crystals, (**3BC**)$_{0.9}$[$(Na^+)_{0.05}$•(**1**)$_{0.1}$•$(PF_6^-)_{0.05}$], (**3BC**)$_{0.9}$[$(K^+)_{0.05}$•(**1**)$_{0.1}$•$(PF_6^-)_{0.05}$], and (**3BC**)$_{0.9}$[$(Cs^+)_{0.05}$•(**1**)$_{0.1}$•$(CO_3^{2-})_{0.025}$], were obtained by mixing **3BC** and **1** in a ratio of 9:1 in toluene and the corresponding M^+X^- in CH_3OH, followed by solvent removal under vacuum and drying.

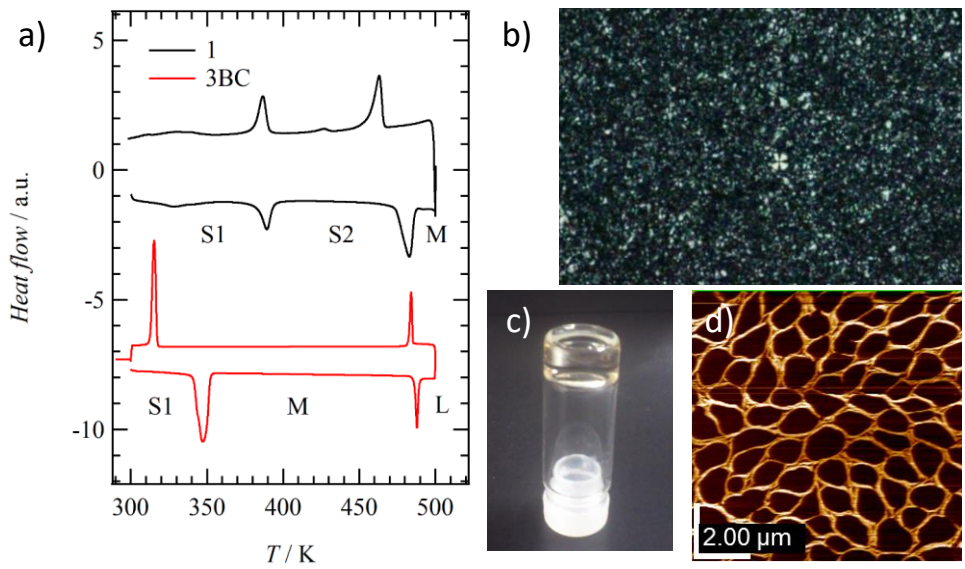

Figure S1. Thermal properties and molecular assembly structures of **1**. a) DSC profiles of **1** (black) and **3BC** (red), where S1, S2, and M denote solid 1, solid 2, and the Col_h liquid crystal phase, respectively. b) POM images of Col_h phase of **1** at 503 K. c) Formation of transparent organogel of **1** in toluene. d) Nanofiber network structure of **1** on a mica surface fabricated by spin-coating at a rotation speed of 2,000 rpm.

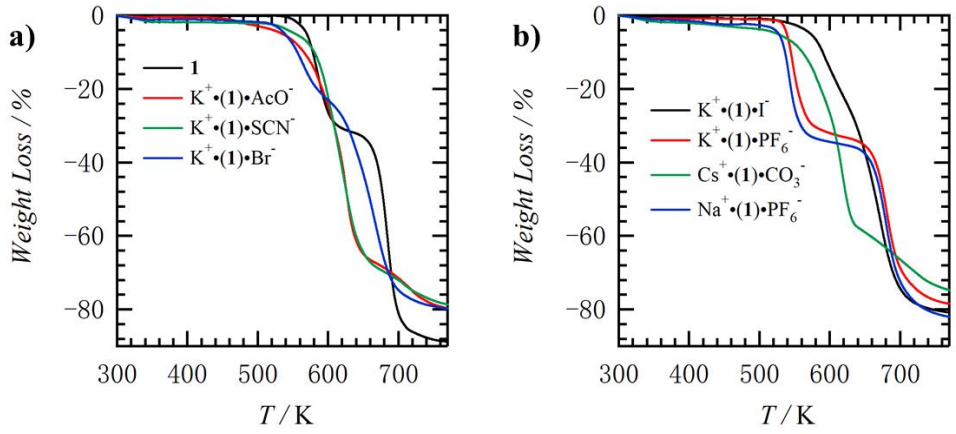

Figure S2. Thermal stability of molecule **1** and **M⁺•(1)•X⁻** salts. a) TG diagrams of molecule **1**, K^+•(**1**)•AcO^-, K^+•(**1**)•SCN^-, K^+•(**1**)•Br^- and K^+•(**1**)•AcO^-. b) TG diagrams of K^+•(**1**)•I^-, K^+•(**1**)•PF_6^-, Cs^+•(**1**)•CO_3^- and Na^+•(**1**)•PF_6^-.

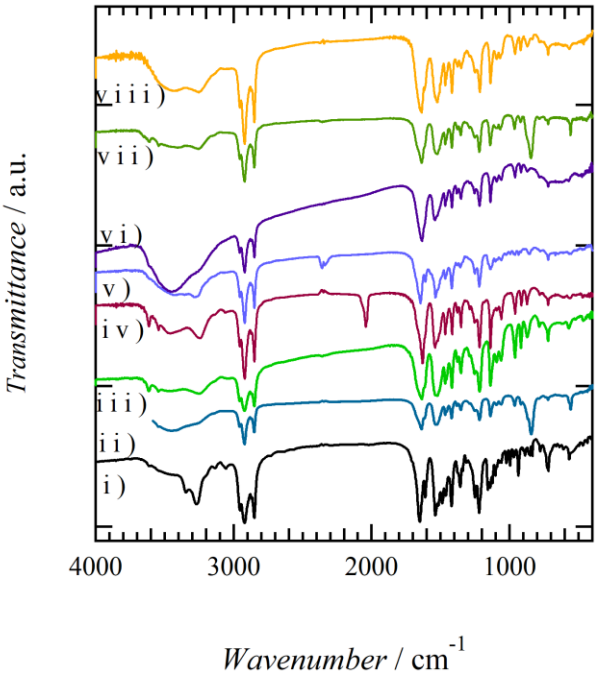

Figure S3. Vibrational IR spectra of molecule **1** and **M⁺•(1)•X⁻** salts on KBr pellets. i) molecule **1**, ii) K^+•(**1**)•PF_6^-, iii) K^+•(**1**)•I^-, iv) K^+•(**1**)•SCN^-, v) K^+•(**1**)•AcO^-, vi) K^+•(**1**)•Br^-, vii) Na^+•(**1**)•PF_6^-, and viii) Cs^+•(**1**)•CO_3^-.

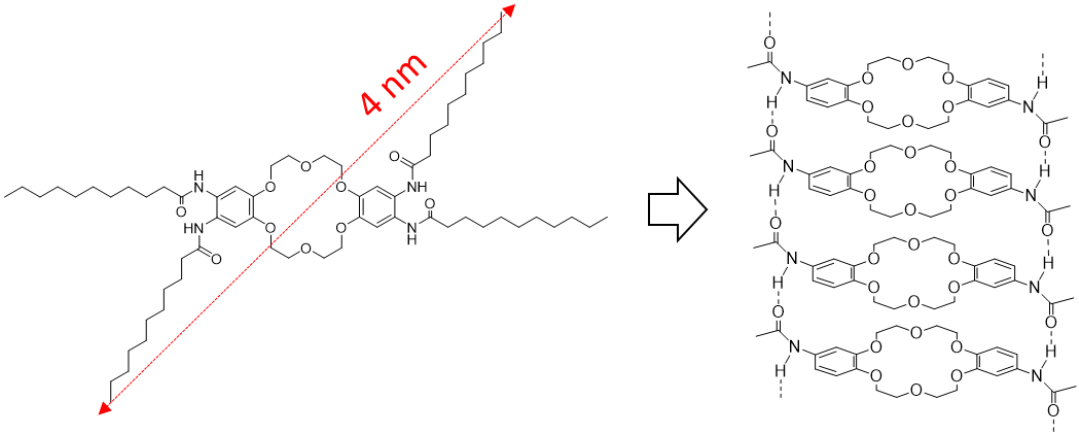

Figure S4. Schematic of the molecular assembly structure of **1**. The maximum molecular length is ~4 nm assuming an all-*trans* conformation of the $–C_{10}H_{21}$ chains (left), which further assembled through =O•••N−H− hydrogen-bonding interaction to form an ionic channel (right). Parts of $–NHCOC_{10}H_{21}$ chains were omitted for clarity.

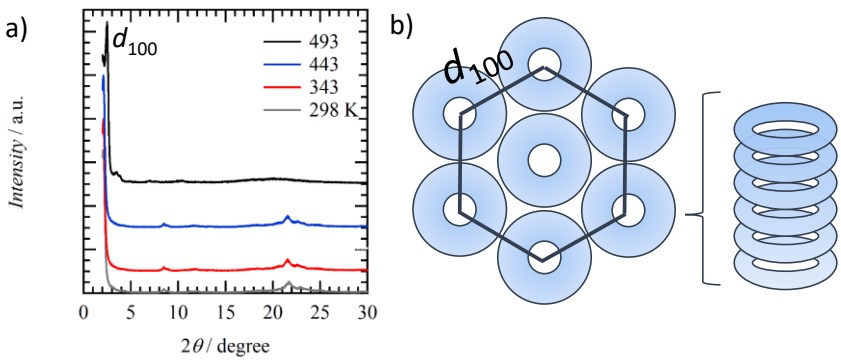

Figure S5. Molecular assembly structure of **1**. a) Temperature-dependent PXRD profiles of S1 (T = 298 and 343 K), S2 (T = 443 K), and Col_h (T = 493 K) phases. b) Schematic model and d_{100} spacing of Col_h phase with an ionic channel structure.

Table S1. Phase transition behaviors of **1** and M^+•(**1**)•X^- salts.

Compounds	Transition [a]	Transition T [b], K	ΔH , kJ mol^{-1}	Mixing [c]
1	S1−S2	382	10.1	–
	S2−Col_h	473	14.1	
	Col_h –I.L.	Dec.	–	
K^+•(**1**)•Br^-	S1−S2	394	3.05	Non.
	S2−Col_h	448	4.13	
	Col_h –I.L.	Dec.	–	
K^+•(**1**)•I^-	S−Col_h	328	24.4	Mix.
	Col_h–I.L.	478	43.6	
K^+•(**1**)•PF_6^-	S−Col_h	334	17.3	
	Col_h–I.L.	Dec.	–	
K^+•(**1**)•AcO^-	S1–S2	354	3.39	Mix.
	S2–Col_h	437	7.68	
	Col_h–I.L.	> 468	1.25	
K^+•(**1**)•SCN^-	S−Col_h	350	1.28	Mix.
	Col_h–I.L.	483	48.8	
Na^+•(**1**)•PF_6^-	S1–S2	340	0.92	Mix.
	S2–Col_h	388	4.36	
	Col_h– I.L.	472	16.0	

Cs^{+}•(**1**)•$(CO_3^{2-})_{0.5}$	S1–S2	362	5.25	Mix.
	S2–Col_h	380	0.81	
	Col_h–I.L.	453	2.28	

[a] S1, S2, Col_h, and I.L. denote low-temperature solid, high-temperature solid, discotic hexagonal columnar, and isotopic liquid phases, respectively. [b] Determined by DSC profiles, and Dec. indicates decomposition without melting behavior. [c] Mixing state of $M^{+}X^{-}$ into **1**. Mix. and Non. denote uniformly mixed and phase-separated states, respectively.

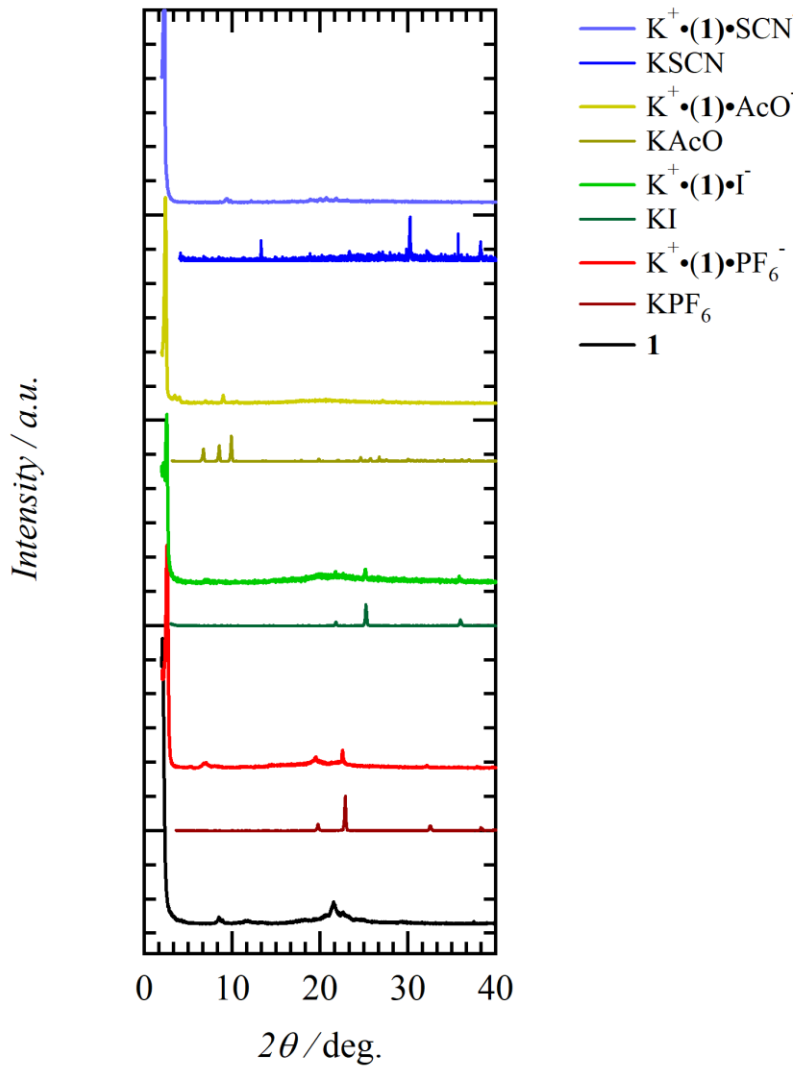

Figure S6. PXRD patterns of Col_h phase of molecular **1**, K^{+}•(**1**)•SCN^{-}, K^{+}•(**1**)•AcO^{-}, K^{+}•(**1**)•I^{-} and K^{+}•(**1**)•PF_6^{-} at 443 K and corresponding salts.

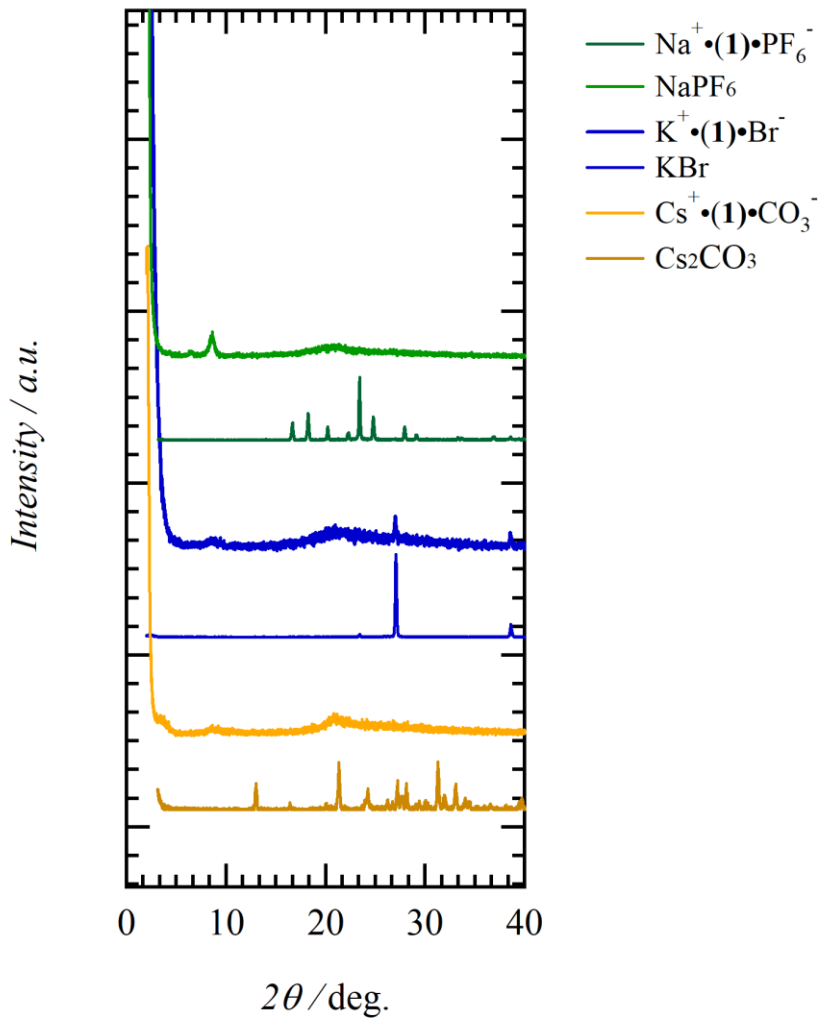

Figure S7. PXRD patterns of Na^{+}•(**1**)•PF_6^{-}, K^{+}•(**1**)•Br^{-} and Cs^{+}•(**1**)•$(CO_3^{2-})_2$ at 300K and corresponding salts.

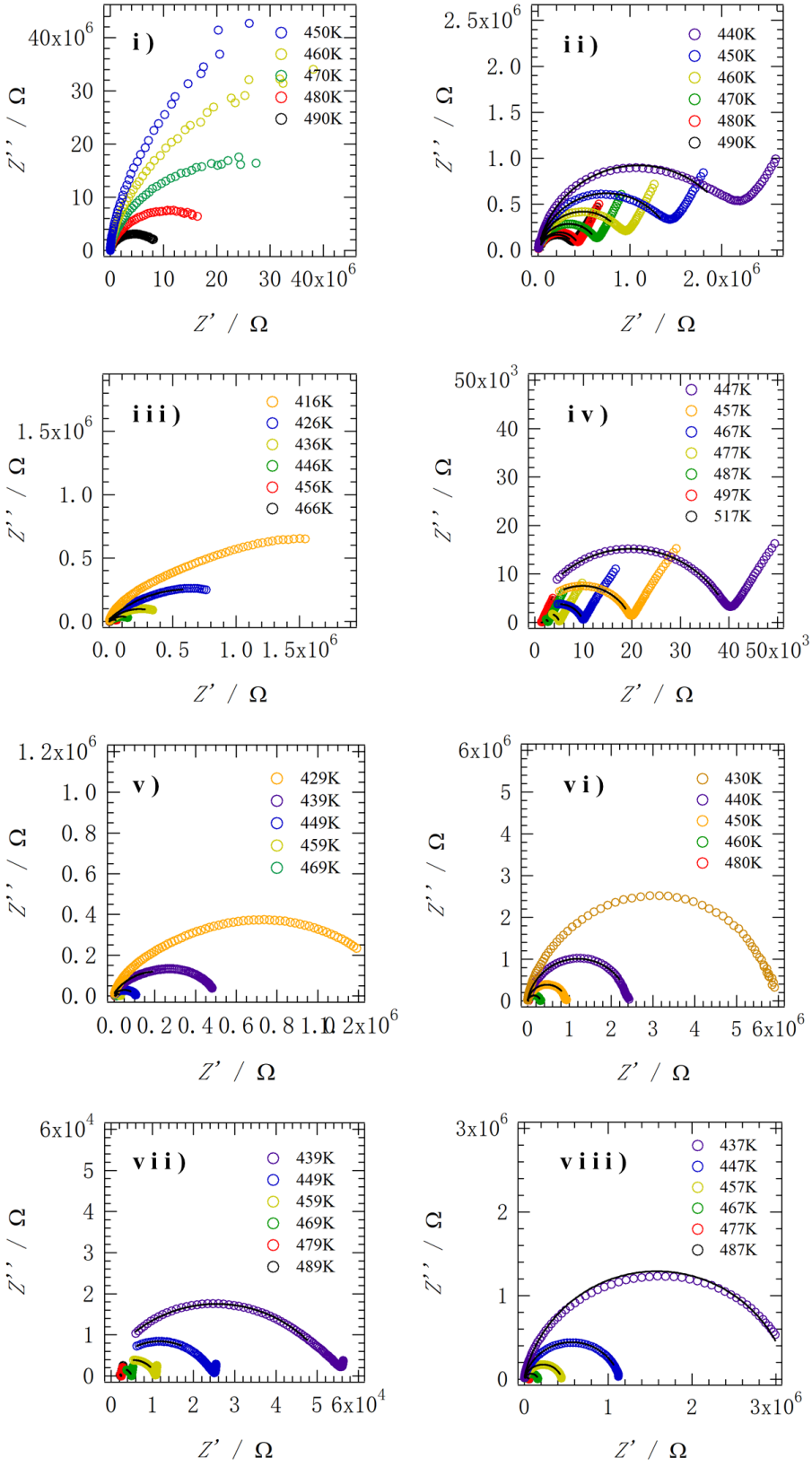

Figure S8. Temperature-dependent *Z'*-*Z''* plots of molecule **1** and **M**$^+$•(**1**)•**X**$^-$ salts. i) molecule **1**, ii) K^+•(**1**)•Br^-, iii) K^+•(**1**)•I^-, iv) K^+•(**1**)•PF_6^-, v) K^+•(**1**)•AcO^-, vi) K^+•(**1**)•SCN^-, vii) Na^+•(**1**)•PF_6^-, and viii) Cs^+•(**1**)•CO_3^-.

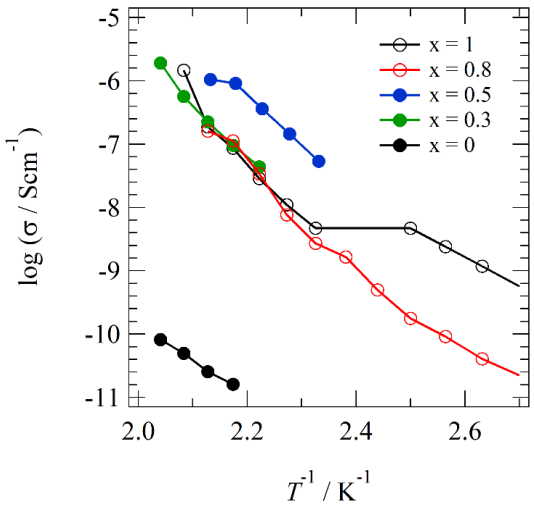

Figure S9. K^+ concentration-dependent $\log(\sigma_{K+})$–T^{-1} plots of $(K^+)_x$•(**1**)•$(SCN^-)_x$ salts with x = 0, 0.3, 0.5, 0.8, and 1.0.

Table S2. Ionic conductivities (σ_{ion}, S cm^{-1}) and activation energies (E_a, eV) of (M^+)•(**1**)•(X^-) salts.

Compound	*T*, K					E_a, eV
	σ_{ion}, S cm^{-1}					
1	490	480	470	460	450	1.07
	8.2×10^{-11}	5.0×10^{-11}	2.5×10^{-11}	1.6×10^{-11}	1.6×10^{-11}	
K^+•(**1**)•Br^-	490	480	470	460	350	0.44~0.63
	2.3×10^{-8}	2.1×10^{-8}	1.4×10^{-8}	9.7×10^{-9}	6.3×10^{-9}	
K^+•(**1**)•AcO^-	469	459	449	439	429	0.13~2.15
	1.7×10^{-6}	7.3×10^{-7}	2.0×10^{-7}	5.2×10^{-8}	1.7×10^{-8}	
K^+•(**1**)•I^-	486 [a]	466	456	446	436	0.54~2.17
	1.5×10^{-5}	5.0×10^{-6}	3.2×10^{-7}	1.2×10^{-7}	5.2×10^{-8}	
K^+•(**1**)•PF_6^-	487	477	467	457	447	0.37~1.26
	6.1×10^{-6}	3.4×10^{-6}	1.7×10^{-6}	8.6×10^{-6}	4.2×10^{-7}	
Na^+•(**1**)•PF_6^-	489 [a]	479 [a]	469	459	449	1.40
	1.7×10^{-5}	1.6×10^{-5}	7.8×10^{-6}	3.6×10^{-6}	1.6×10^{-6}	
Cs^+•(**1**)•$(CO_3^{2-})_{0.5}$	487 [a]	477 [a]	467 [a]	457	447	1.70
	5.9×10^{-7}	6.1×10^{-7}	2.0×10^{-7}	7.3×10^{-8}	2.9×10^{-8}	
K^+•(**1**)•SCN^-	480	470	460	450	440	1.64
	1.5×10^{-6}	1.9×10^{-7}	8.6×10^{-8}	2.9×10^{-8}	1.1×10^{-8}	
$(K^+)_{0.8}$•(**1**)•$(SCN^-)_{0.8}$	470	460	450	440	430	0.82~1.90
	1.0×10^{-6}	7.0×10^{-7}	2.1×10^{-7}	4.8×10^{-8}	1.7×10^{-8}	
$(K^+)_{0.5}$•(**1**)•$(SCN^-)_{0.5}$	469	459	449	439	329	1.60
	5.0×10^{-6}	9.2×10^{-7}	3.7×10^{-7}	1.4×10^{-7}	5.4×10^{-7}	
$(K^+)_{0.3}$•(**1**)•$(SCN^-)_{0.3}$	490 [a]	480	470	460	450	1.59
	1.9×10^{-6}	5.7×10^{-7}	2.2×10^{-7}	9.5×10^{-8}	4.4×10^{-8}	

[a] Ionic conductivity in the I.L. phase.

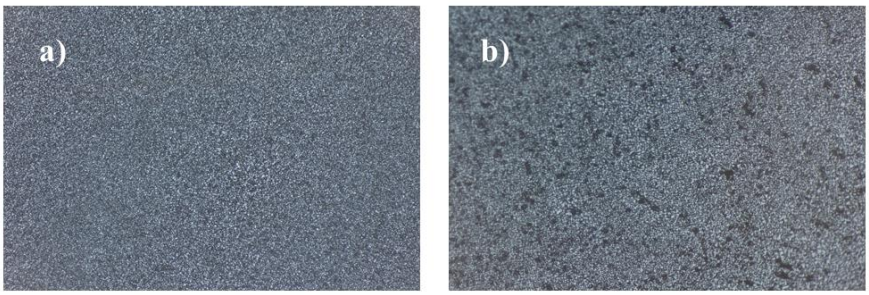

Figure S10. POM Images of a) $(\mathbf{3BC})_{0.8}(\mathbf{1})_{0.2}$ and b) $(\mathbf{3BC})_{0.7}(\mathbf{1})_{0.3}$

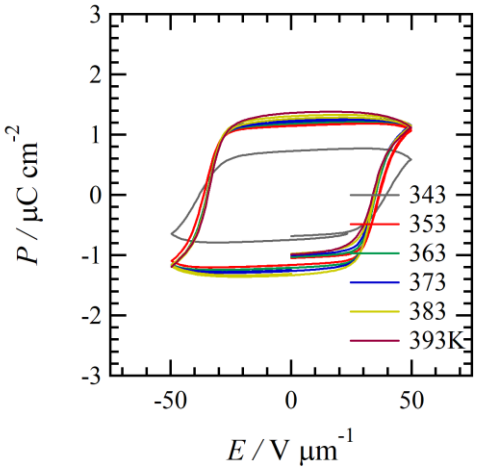

Figure S11. Temperature-dependent *P*−*E* hysteresis curves of **3BC**.

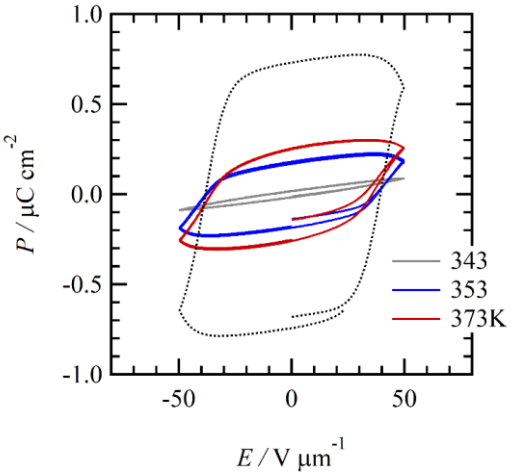

Figure S12. Temperature-dependent *P*−*E* hysteresis curves of $\mathrm{Col_h}$ phases for mixed crystals $(\mathbf{3BC})_{0.8}(\mathbf{1})_{0.2}$.